Supplementary Online Content

Hauser TU, Iannaccone R, Ball J, et al. Role of the medial prefrontal cortex in impaired decision making in juvenile attention-deficit/hyperactivity disorder.
JAMA Psychiatry. Published online August 20, 2014.
doi:10.1001/jamapsychiatry.2014.1093.

This supplementary material has been provided by the authors to give readers additional information about their work.

© 2014 American Medical Association. All rights reserved.

Downloaded From: http://archpsyc.jamanetwork.com/ by a ETH ZUERICH User on 04/22/2016

eMethods. Supplementary Methods

Probabilistic reversal learning task

The task was similar to the task described in Hauser et al.(2014)[1]. On each trial, the subjects had to select the one of two stimuli. One of the two stimuli had a reward probability of 0.8 while the other stimulus had a reward probability of only 0.2. The subjects had to learn the reward probabilities on a trial-and-error basis. After six to 10 correct (minimally three consecutive correct responses) responses, the reward probabilities reversed, to which the subjects then had to adapt. The participants knew about the possibility of reversal, but they were not informed about any details of the reversals. Rewards were depicted by a framed 50 Swiss Centimes coin. As punishment, the participants lost 50 Swiss Centimes. The task consisted of two runs with 60 trials each. Participants were instructed to win as much money as possible. They knew that half of the money won was paid to them at the end of the study. On each trial, two objects were presented for 1500ms. One of the stimuli (the "correct" stimulus) had a reward probability of 0.8 and a punishment probability of 0.2. The other, "incorrect" stimulus had a punishment probability of 0.8 and a win probability of 0.2. Late answers (>1500ms) were punished with one Swiss Franc. This was done to prevent late answers and these trials did not enter the learning analysis. The average total trial duration was 9000ms. In each run, we additionally presented 20 null trials of 9000ms length.

Computational models

To infer behavior, we tested two learning models and two decision models. We performed model comparison using Bayesian random effects analysis[2]. The best performing model combination over all participants was used for group comparison and further analyses.

To ensure that participants did not respond randomly, performing at chance level, we additionally built a simple model without any free parameter which always resulted in a choice probability of 0.5 at every trial. This chance model was compared to the best performing of the other models. If the chance model performed equally well or better, we excluded this subject from analysis, given that no learning was detectable.

Learning models

We compared two different models which are explained in what follows. Note that, for clarity, we use δ for the RPE during outcome and choice value $V_{chosen}^{(t)}$ for RPE during cue presentation (because RPE_{cue} is the difference between the expected value of the cue and not presenting a cue, which equals zero). For a more detailed explanation of this notational choice, see e.g., Niv et al. (2012)[3]. In the results and discussion sections, we use RPE_{cue} for the expected value (V_{chosen}) and $RPE_{outcome}$ for δ.

Anticorrelated Rescorla-Wagner model

δ at each trial t was computed as the difference between the anticipated ($V_{chosen}^{(t)}$) and the received ($R^{(t)}$) outcome:

$$\delta^{(t)} = R^{(t)} - V_{chosen}^{(t)} \quad (1)$$

The values of both options were then updated using δ[4]:

$$V_{chosen}^{(t+1)} = V_{chosen}^{(t)} + \alpha\delta^{(t)} \quad (2)$$

$$V_{unchosen}^{(t+1)} = V_{unchosen}^{(t)} - \alpha\delta^{(t)}, \quad (3)$$

where α depicts the learning rate. The priors for the model fitting procedure were set to $V^{(0)} = .5$, $\alpha = .5(10)$ (mean(variance in logit space)).

Hierarchical Gaussian Filter model (HGF)

The HGF is a generic hierarchical, approximately Bayes-optimal learning model. The HGF fully complies with the assumptions of predictive coding and the Bayesian brain hypothesis, which states that the brain always learns in a Bayes-optimal fashion, given individually different priors[5,6]. The exact formulation, the model inversion and the complete update equations are described in Mathys et al. (2011)[7–9]. The HGF, as used here, consists of a hierarchy of 3 hidden states, where the states at levels 2 and 3 (x_2, x_3, resp.) evolve as Gaussian random walks over time (Figure 1B). x_1 ($\in \{0,1\}$) indicates the environmental state that defines which stimulus is being rewarded. It is governed by the state x_2 ($\in \{-\infty\infty\}$), which is transformed to the probability that x_1 by a logistic sigmoid transformation

© 2014 American Medical Association. All rights reserved.

Downloaded From: http://archpsyc.jamanetwork.com/ by a ETH ZUERICH User on 04/22/2016

$$p(x_1^{(t)} \mid x_2^{(t)}) = s(x_2^{(t)})^{x_1^{(t)}} (1 - s(x_2^{(t)}))^{1 - x_1^{(t)}} \tag{4}$$

with $s(x) := (1/(1+e^{-x}))$. State x_2 evolves over time and is determined by a Gaussian random walk. The value of $x_2^{(t)}$ is normally distributed with mean $x_2^{(t-1)}$ and variance $e^{\kappa x_3^{(t)} + \omega}$

$$p(x_2^{(t)}) \sim N(x_2^{(t-1)}, e^{\kappa x_3^{(t)} + \omega}) \tag{5}$$

Since the variance of this random walk can be taken as a measure of the volatility of x_2, the log-volatility $\kappa x_3^{(t)} + \omega$ has two components, one phasic and the other tonic: x_3 is a state-dependent (phasic) log-volatility, while ω is a free parameter defining a subject-specific (tonic) log-volatility. κ was fixed to 1 as in Vossel et al. (2013)[8]. The state $x_3^{(t)}$ is normally distributed with mean $x_3^{(t-1)}$ and variance ϑ. ϑ is a free parameter and can be regarded as a subject-specific meta-volatility.

$$p(x_3^{(t)}) \sim N(x_3^{(t-1)}, \vartheta) \tag{6}$$

The variational inversion of the model yields subject-specific Gaussian belief trajectories about x_2 and x_3, represented by their means μ_2, μ_3 and variances (or, equivalently, precisions) σ_2, σ_3 (π_2, π_3). This inversion revealed that the trial-by-trial update equations highly resemble the update equations from Rescorla-Wagner models (cf. equation 1):

$$\delta_1^{(t)} = R^{(t)} - s(\hat{\mu}_2^{(t)}), \tag{7}$$

where $\hat{\mu}_2^{(t)} = \mu_2^{(t-1)}$ is the trial-by-trial mean of the Gaussian prior at the second level and $R^{(t)} := x_1^{(t)}$. $\hat{\mu}_2^{(t)}$ is updated by a precision-weighted RPE

$$\hat{\mu}_2^{(t+1)} = \mu_2^{(t)} = \hat{\mu}_2^{(t)} + \sigma_2^{(t)} \delta_1^{(t)}, \tag{8}$$

where $\sigma_2^{(t)}$ is the trial-by-trial variance at level 2. It can be expressed by a ratio of precision estimates $\hat{\pi}$

$$\sigma_2^{(t)} = \frac{\hat{\pi}_1^{(t)}}{\hat{\pi}_2^{(t)} \hat{\pi}_1^{(t)} + 1}, \tag{9}$$

$$\hat{\pi}_2^{(t)} := \frac{1}{\sigma_2^{(t-1)} + e^{\mu_3^{(t-1)} + \omega}}, \tag{10}$$

$$\hat{\pi}_1^{(t)} := \frac{1}{s(\mu_2^{(t-1)})(1 - s(\mu_2^{(t-1)}))} \tag{11}$$

For the update equations at level 3 and for the derivation of the equations, please refer to Mathys et al. (2011)[7]. Parameters were estimated in spaces where they were unbounded (e.g., the initial values σ_0 of the variances were estimated in logarithmic space, where their possible values are unbounded, while in native space there is a lower bound at zero). This enabled the use of Gaussian priors, which (in the appropriate spaces) were set to μ_0=[0,1](0,0), σ_0=[0,0](1,1), κ=1(0), ω=-2(10), ϑ=.03(1).

To sum up, the HGF has a similar update structure as the anticorrelated Rescorla-Wagner model (cf. equations 1 and 2 with 7 and 8). But instead of a fixed learning rate across the whole experiment (i.e., α), the learning rate is determined by an estimate of the variance of the belief (eq. 9). Therefore, the impact of the RPEs (δ_1) is modulated by the environmental volatility and the certainty of beliefs, resulting in a bigger impact of RPEs in more uncertain trials.

For a better understanding of this model in the context of RPE-theories, we define $\hat{\mu}_2^{(t)}$ of the chosen object as the choice value ($V_{chosen}^{(t)}$) and δ_1 as RPE. We decided not to investigate higher-order updates and beliefs because we had no specific hypotheses about these levels of the model.

Decision models

© 2014 American Medical Association. All rights reserved.

Downloaded From: http://archpsyc.jamanetwork.com/ by a ETH ZUERICH User on 04/22/2016

We combined each of the learning models with two of the most commonly used decision models. As first model, we chose a softmax function,

$$p(A) = \frac{1}{1 + e^{-\beta(V_A - V_B)}}, \tag{12}$$

where $p(A)$ denotes the probability of choosing object A and β is a free parameter. As a second decision model, we implemented a unit square sigmoid transformation

$$p(A) = \frac{V_A^{\xi}}{V_A^{\xi} + V_B^{\xi}}, \tag{13}$$

where ξ denotes the free parameter.

The main difference between these two models is how they translate beliefs into action probabilities. The softmax model is more flexible, especially in decisions with beliefs of high certainty, where the unit square model is (almost) deterministic. So far, the softmax model has mainly been used to model reversal learning tasks[1,4,10]. Nevertheless, with this comparison, we wanted to ensure that this decision model is also well suited for our data.

Model fitting procedure

All models were implemented and estimated using the HGF toolbox framework (v2.1; http://www.translationalneuromodeling.org/tapas/). We used the (negative) variational free-energy F to compare the model fits. F is a lower bound on the log-model-evidence, and the maximization of F therefore minimizes the Kullback-Leibler divergence between the exact and the approximate posterior distribution[11]. For optimization, we used the Broyden, Fletcher, Goldfarb and Shanno (BFGS) quasi-Newton optimization algorithm. We compared each combination of a learning model with a decision model using Bayesian model selection (BMS)[2]. Because the two groups could have had a different winning model, we ran BMS for all subjects together as well as for each group independently.

Data acquisition

We recorded fMRI in a 3 T Philips Achieva Scanner (Philips Medical Systems, Best, the Netherlands), which was equipped with a receive-only 32-element head coil array. We used an echo planar imaging (EPI) sequence which was optimized for maximal orbitofrontal signal sensitivity (TR: 1850ms, TE: 20ms, 15° tilted downwards of AC-PC, 40 slices, 2.5*2.5*2.5mm voxels, 0.7mm gap, FA: 85° FOV: 240*240*127mm). For normalization purposes we also acquired a T1-weighted structural image. For our simultaneous EEG acquisition, we used two MR-compatible 32-channel DC amplifiers (BrainProducts GmbH, Gilching, Germany). We recorded the data with a sampling rate of 5 kHz (recording reference: Fz, EEG recording filters: DC-250 Hz, ECG: DC-1000 Hz) from 63 scalp electrodes and 2 ECG channels. The 63 scalp electrodes covered the international 10-20-system[12] plus the following positions: FPz, AFz, AF2, FCz, CPz, POz, Oz, Iz, F5/6, FC1/2/3/4/5/6, FT7/8/9/10, C1/2/5/6, CP1/2/3/4/5/6, TP7/8/9/10, P5/6, PO1/2/9/10, OI1/2, left and right eye (laterally and below the eyes). For a more even coverage, O1'/2' and FP1'/2' were located 15% more laterally to Oz/FPz.

fMRI analysis

For fMRI preprocessing and analysis, we used SPM8 (http://www.fil.ion.ucl.ac.uk/spm/). The raw data were realigned, resliced, and coregistered to the T1 image. For normalization, the deformation fields were used, which were obtained using new segmentation. This procedure resulted in a new standard voxel size of 1.5*1.5*1.5mm. Subsequently, the data were spatially smoothed (6mm FWHM kernel).

For our fMRI analysis, we estimated the RPEs and choice values using the winning model across all participants. In the first-level GLM, we entered the model-derived RPEs ($RPE_{outcome}$, here δ_1) at feedback onset and choice values (RPE_{cue}, here $\hat{\mu}_2$) at cue presentation as parametric modulators. Additionally, we entered the following regressors of no interest to improve model validity. To control for movement-induced effects, we entered the realignment-derived movement parameters. Furthermore, we entered an additional regressor for each scan with a scan-to-scan motion > 1mm (determined using a custom adaptation of the artRepair-toolbox, http://cibsr.stanford.edu/tools/human-brain-project/artrepair-software.html). Because the heart rate is known to differ between ADHD and controls in reinforcement paradigms[13] and because pulsations induce micro-movements and therefore add noise to the data, we additionally regressed out pulsatile effects using an adaptation of RETROICOR (http://www.translationalneuromodeling.org/tapas/)[14,15]. Missing answers were also entered into a regressor-of-no-interest. For all task-related regressors, the spatial and temporal derivatives were enabled. Results of the random-

© 2014 American Medical Association. All rights reserved.

Downloaded From: http://archpsyc.jamanetwork.com/ by a ETH ZUERICH User on 04/22/2016

effects fMRI analyses are reported using a p<.05 voxel-height FWE threshold for task main effects, and p<.05 cluster-extent FWE correction (voxel-height threshold p<.001) for between group comparisons.

RPE main effects and group differences
To analyze the neural correlates of RPE processing during cue presentation and outcome (task main effects), we entered all subjects into one random effects analysis. To obtain the group differences, we compared both groups using independent t-tests (separately for RPE_{cue} and $RPE_{outcome}$).

Neural correlates of β
We evaluated where in the brain the decision steepness (model parameter β) is processed. To do so, we ran a covariate analysis during cue presentation with β as covariate in all subjects. To eliminate between-group effects, we added the group as an additional covariate-of-no-interest.

ROI-Analysis of sgACC/VS-cluster
ADHD – in particular with respect to decision making – has often been associated with activation differences in the ventral striatum[16]. We therefore decided to investigate the activity in this area, which is well known for processing RPEs[17–19]. In our RPE main effects analysis (RPE_{cue} and $RPE_{outcome}$ combined), we found a significant cluster containing the subgenual ACC and ventral striatum (sgACC/VS) to be activated by RPEs (cf. eFigure 2, 3E, eTable 3). We defined the ROI (8mm sphere) based on the peak voxel in the sgACC/VS cluster of our task main effects analysis (eFigure 2A, eTable 3). The effects of RPEs were computed using rfxplot[20]. We performed a split-half analysis of the RPE trials (hereafter: positive and negative RPEs) and used repeated measures ANOVAs and post hoc t-tests to compare the RPEs. The same analysis was also conducted based on a peak voxel from an independent group of healthy adults (n=25, 29.9y±7.4, 16m/9f) which played the same task. Their data were analyzed in the same way as described above. We also found a strongly significant main effects RPE activation in the sgACC/VS area (MNI: x=-5, y=17, z=-14; t(24)=6.53) and used this peak as the center of the ROI.

Functional connectivity analysis
To better understand how the impairments in the mPFC can be related to the sgACC/VS-impairment, we performed an exploratory connectivity analysis. We entered the SPM-derived first-level GLMs into the CONN-fMRI functional connectivity toolbox (v13p, http://www.nitrc.org/projects/conn/). Additionally, we entered the segmented structural images (gray matter, white matter, cerebro-spinal fluid) into the analysis for additional motion correction. The data were filtered using .008-.09Hz bandpass filter and we performed a ROI-to-ROI functional connectivity analysis (bivariate regression) using the mPFC clusters which were found to be impaired in the main RPE analysis. Additionally, the sgACC/VS-ROI was entered.

EEG preprocessing, analysis, and source localization
We used BrainVision Analyzer 2.0.2 (BrainProducts GmbH, Gilching, Germany) for EEG preprocessing. MR artifact correction was conducted using sliding average subtraction[21]. Cardioballistic artifacts were removed using the implemented CBC correction algorithms. The data was resampled (256 Hz) and filtered (.1 Hz-30 Hz, 50 Hz notch). Ocular and remaining cardioballistic artifacts were excluded using independent component analysis (ICA). The continuous data was re-referenced to average reference[22] and then exported for further analysis to Matlab using the eeglab-toolbox[23].
We used a peak-to-peak analysis to define the FRN. We segmented (-100-700ms relative to feedback onset) and baseline-corrected (-100-0ms) the continuous data in reward and punishment trials separately. Epochs with amplitudes greater than ±80μV were excluded from subsequent analyses (number of trials excluded: ADHD: 21±26, controls: 15±17, t(36)=.81, p=.426). We restricted our analysis to the electrodes Cz, FCz, and Fz, which are most often used in FRN analyses. For each subject, we determined the most negative peak between 200-425ms (punishment: ADHD: 316ms±43, controls: 323ms±46, t(36)=.43, p=.670; reward: ADHD 339ms±34, controls: 331ms±38, t(36)=-.71, p=.485) and the most positive preceding peak between 150-300ms (punishment: ADHD: 203ms±34, controls: 206ms±34, t(36)=.28, p=.780; reward: ADHD: 213ms±30, controls: 208ms±32, t(36)=-.55, p=.589), similar to the study by Zottoli and Grose-Fifer (2012)[24]. To determine the electrode with the maximal feedback-related response, we selected the electrode with the biggest difference between the two peaks. For both groups, electrode Fz elicited the biggest feedback-related response (Cz: $controls_{reward}$: -5.15μV±2.47, $controls_{punishment}$: -4.82μV±2.51, $ADHD_{reward}$: -5.63μV±3.23, $ADHD_{punishment}$: -5.15μV±2.65; FCz: $controls_{reward}$: -6.46μV±2.68, $controls_{punishment}$: -6.66μV±3.27, $ADHD_{reward}$: -7.53μV±3.67, $ADHD_{punishment}$: -6.54μV±3.60; Fz: $controls_{reward}$: -8.06μV±3.04, $controls_{punishment}$: -9.74μV±3.90, $ADHD_{reward}$: -8.81μV±4.08, $ADHD_{punishment}$: -

© 2014 American Medical Association. All rights reserved.

Downloaded From: http://archpsyc.jamanetwork.com/ by a ETH ZUERICH User on 04/22/2016

8.21μV±4.55, eFigure 2). We calculated the FRN by subtracting rewards from punishments and compared the FRN between the groups using independent t-tests.

To localize the FRN, we took the single-trial amplitudes and used them as a parametric modulator at the time of feedback in the first-level fMRI-GLM. We additionally entered all the regressors mentioned above (with exception of $RPE_{outcome}$) to improve model fit. We set the significance level to $p<.001$ cluster-extent FWE correction (voxel-height threshold $p<.005$) and localized the FRN in both groups independently.

© 2014 American Medical Association. All rights reserved.

Downloaded From: http://archpsyc.jamanetwork.com/ by a ETH ZUERICH User on 04/22/2016

eResults. Supplementary Results

Neural correlates of RPE processing: main effects

When analyzing the main effect of RPEs (cue and outcome combined), we found a network which showed increasing activation with increasing RPEs containing the ventromedial prefrontal cortex (vmPFC), posterior cingulate cortex (PCC), amygdala, lateral prefrontal cortex (latPFC), and a cluster containing the subgenual anterior cingulate cortex and the ventral striatum (sgACC/VS; eFigure 2A, eTable 3). A network containing the anterior insula, mPFC, latPFC, dorsolateral prefrontal cortex (dlPFC), inferior parietal lobe (IPL), precuneus, caudate, midbrain, and thalamus showed increasing activation with decreasing RPEs (eFigure 2B, eTable 3). For the RPE effects separated for cue and outcome, please refer to Figure 2.

Neural correlates of the decision steepness

Because we found differences in our model parameter β which indicates the steepness of the decision function (i.e. how exploratorily a subject behaves), we wanted to determine its neural correlates. Our covariate analysis revealed a network which contains mPFC, latPFC, dlPFC, STG and precentral area (eFigure 2C-D, eTable 3). These regions are well known regions of the decision making network: especially the mPFC has been associated with value comparison and response selection[25–27].

Analysis of sgACC/VS-ROI

The analysis of our sgACC/VS-ROI revealed a significant RPE (negative, positive) * time (cue, outcome) * group (ADHD, controls) interaction ($F(1,36)=6.16$, $p=.018$). Post hoc t-tests revealed that there was no difference for RPE_{cue} (negative RPE: $t(36)=.17$, $p=.865$; positive RPE $t(36)=-.15$, $p=.883$, eFigure 3A). For $RPE_{outcome}$, there was a significant difference for negative ($t(36)=-2.83$, $p=.007$, eFigure 3B) and positive RPEs ($t(36)=2.84$, $p=.007$). Also for the analysis which was based on an independent adult sample (s. above), we found a significant RPE (negative, positive) * time (cue, outcome) * group (ADHD, controls) interaction ($F(1,36)=5.17$, $p=.029$). Post hoc t-tests revealed that there was no difference for RPE_{cue} (negative RPE: $t(36)=.070$, $p=.945$; positive RPE $t(36)=-.065$, $p=.949$, eFigure 3C). For $RPE_{outcome}$, there was a significant difference for negative ($t(36)=-2.55$, $p=.015$, eFigure 3D) and positive RPEs ($t(36)=2.54$, $p=.015$). Thus, both groups showed similar RPE activation patterns during cue presentation, but controls show stronger RPE activation than subjects with ADHD in the sgACC/VS during outcome.

Functional connectivity analysis

To understand whether the differences between the mPFC were related to the sgACC/VS-cluster, we performed a ROI-to-ROI connectivity analysis. We found a significant connectivity in both groups between $mPFC_{outcome}$ and the sgACC/VS (controls: .326±.147, $t(19)=9.91$, $p<.001$; ADHD: .192±.137, $t(17)=5.95$, $p<.001$; eFigure 3E) and between the $mPFC_{outcome}$ and $mPFC_{cue}$ (controls: .395±.399, $t(19)=4.43$, $p<.001$; ADHD: .311±.377, $t(17)=3.50$, $p=.003$). No significant connectivity was found between $mPFC_{cue}$ and sgACC/VS (controls: .134±.467, $t(19)=1.28$, $p=.214$; ADHD: .126±.357, $t(17)=1.49$, $p=.154$). A comparison between the groups revealed a significantly reduced connectivity in ADHD between the $mPFC_{outcome}$ and the sgACC/VS ($t(36)=2.89$, $p=.006$), but not in the other two comparisons ($mPFC_{outcome}$-$mPFC_{cue}$: $t(36)=.67$, $p=.510$; $mPFC_{cue}$-sgACC/VS: $t(36)=.06$, $p=.950$).

References

1. Hauser TU, Iannaccone R, Stämpfli P, et al. The Feedback-Related Negativity (FRN) revisited: New insights into the localization, meaning and network organization. *NeuroImage*. 2014;84:159-168.
2. Stephan KE, Penny WD, Daunizeau J, Moran RJ, Friston KJ. Bayesian model selection for group studies. *NeuroImage*. 2009;46(4):1004-1017. doi:10.1016/j.neuroimage.2009.03.025.
3. Niv Y, Edlund JA, Dayan P, O'Doherty JP. Neural prediction errors reveal a risk-sensitive reinforcement-learning process in the human brain. *J Neurosci Off J Soc Neurosci*. 2012;32(2):551-562. doi:10.1523/JNEUROSCI.5498-10.2012.
4. Gläscher J, Hampton AN, O'Doherty JP. Determining a role for ventromedial prefrontal cortex in encoding action-based value signals during reward-related decision making. *Cereb Cortex*. 2009;19(2):483-495. doi:10.1093/cercor/bhn098.
5. Dayan P, Hinton GE, Neal RM, Zemel RS. The Helmholtz machine. *Neural Comput*. 1995;7(5):889-904.
6. Friston KJ. The free-energy principle: a unified brain theory? *Nat Rev Neurosci*. 2010;11(2):127-138. doi:10.1038/nrn2787.
7. Mathys C, Daunizeau J, Friston KJ, Stephan KE. A bayesian foundation for individual learning under uncertainty. *Front Hum Neurosci*. 2011;5:39. doi:10.3389/fnhum.2011.00039.

© 2014 American Medical Association. All rights reserved.

Downloaded From: http://archpsyc.jamanetwork.com/ by a ETH ZUERICH User on 04/22/2016

8. Vossel S, Mathys C, Daunizeau J, et al. Spatial Attention, Precision, and Bayesian Inference: A Study of Saccadic Response Speed. *Cereb Cortex N Y N 1991*. 2013. doi:10.1093/cercor/bhs418.
9. Joffily M, Coricelli G. Emotional Valence and the Free-Energy Principle. *PLoS Comput Biol*. 2013;9(6):e1003094. doi:10.1371/journal.pcbi.1003094.
10. Hampton AN, Bossaerts P, O'Doherty JP. The role of the ventromedial prefrontal cortex in abstract state-based inference during decision making in humans. *J Neurosci*. 2006;26(32):8360-8367. doi:10.1523/JNEUROSCI.1010-06.2006.
11. Friston KJ, Mattout J, Trujillo-Barreto N, Ashburner J, Penny W. Variational free energy and the Laplace approximation. *NeuroImage*. 2007;34(1):220-234. doi:10.1016/j.neuroimage.2006.08.035.
12. Jasper HH. The ten-twenty electrode system of the international federation. *Electroencephalogr Clin Neurophysiol*. 1958;10:370-375.
13. Luman M, Oosterlaan J, Hyde C, van Meel CS, Sergeant JA. Heart rate and reinforcement sensitivity in ADHD. *J Child Psychol Psychiatry*. 2007;48(9):890-898. doi:10.1111/j.1469-7610.2007.01769.x.
14. Kasper L, Marti S, Vannesjö SJ, et al. Cardiac Artefact Correction for Human Brainstem fMRI at 7 Tesla. In: *Proc Org Hum Brain Mapp*.; 2009.
15. Glover GH, Li T-Q, Ress D. Image-based method for retrospective correction of physiological motion effects in fMRI: RETROICOR. *Magn Reson Med*. 2000;44(1):162–167. doi:10.1002/1522-2594(200007)44:1<162::AID-MRM23>3.0.CO;2-E.
16. Plichta MM, Scheres A. Ventral-striatal responsiveness during reward anticipation in ADHD and its relation to trait impulsivity in the healthy population: a meta-analytic review of the fMRI literature. *Neurosci Biobehav Rev*. 2014;38:125-134. doi:10.1016/j.neubiorev.2013.07.012.
17. Gläscher J, Daw N, Dayan P, O'Doherty JP. States versus rewards: Dissociable neural prediction error signals underlying model-based and model-free reinforcement learning. *Neuron*. 2010;66(4):585-595. doi:10.1016/j.neuron.2010.04.016.
18. Rutledge RB, Dean M, Caplin A, Glimcher PW. Testing the reward prediction error hypothesis with an axiomatic model. *J Neurosci Off J Soc Neurosci*. 2010;30(40):13525-13536. doi:10.1523/JNEUROSCI.1747-10.2010.
19. Pessiglione M, Seymour B, Flandin G, Dolan RJ, Frith CD. Dopamine-dependent prediction errors underpin reward-seeking behaviour in humans. *Nature*. 2006;442(7106):1042-1045. doi:10.1038/nature05051.
20. Gläscher J. Visualization of group inference data in functional neuroimaging. *Neuroinformatics*. 2009;7(1):73-82. doi:10.1007/s12021-008-9042-x.
21. Allen PJ, Josephs O, Turner R. A method for removing imaging artifact from continuous EEG recorded during functional MRI. *NeuroImage*. 2000;12(2):230-9. doi:10.1006/nimg.2000.0599.
22. Lehmann D, Skrandies W. Reference-free identification of components of checkerboard-evoked multichannel potential fields. *Electroencephalogr Clin Neurophysiol*. 1980;48(6):609-621.
23. Delorme A, Makeig S. EEGLAB: an open source toolbox for analysis of single-trial EEG dynamics including independent component analysis. *J Neurosci Methods*. 2004;134(1):9-21. doi:10.1016/j.jneumeth.2003.10.009.
24. Zottoli TM, Grose-Fifer J. The feedback-related negativity (FRN) in adolescents. *Psychophysiology*. 2012;49(3):413-420. doi:10.1111/j.1469-8986.2011.01312.x.
25. Hare TA, Schultz W, Camerer CF, O'Doherty JP, Rangel A. Transformation of stimulus value signals into motor commands during simple choice. *Proc Natl Acad Sci U S A*. 2011;108(44):18120-18125. doi:10.1073/pnas.1109322108.
26. Holroyd CB, Coles MGH. The neural basis of human error processing: reinforcement learning, dopamine, and the error-related negativity. *Psychol Rev*. 2002;109(4):679-709.
27. Kennerley SW, Behrens TEJ, Wallis JD. Double dissociation of value computations in orbitofrontal and anterior cingulate neurons. *Nat Neurosci*. 2011;14(12):1581-1589. doi:10.1038/nn.2961.

© 2014 American Medical Association. All rights reserved.

Downloaded From: http://archpsyc.jamanetwork.com/ by a ETH ZUERICH User on 04/22/2016

eFigure 1. Analysis of the FRN.

The FRN was computed as the difference of the amplitude difference between N2 and P2 peak between punishments and rewards.

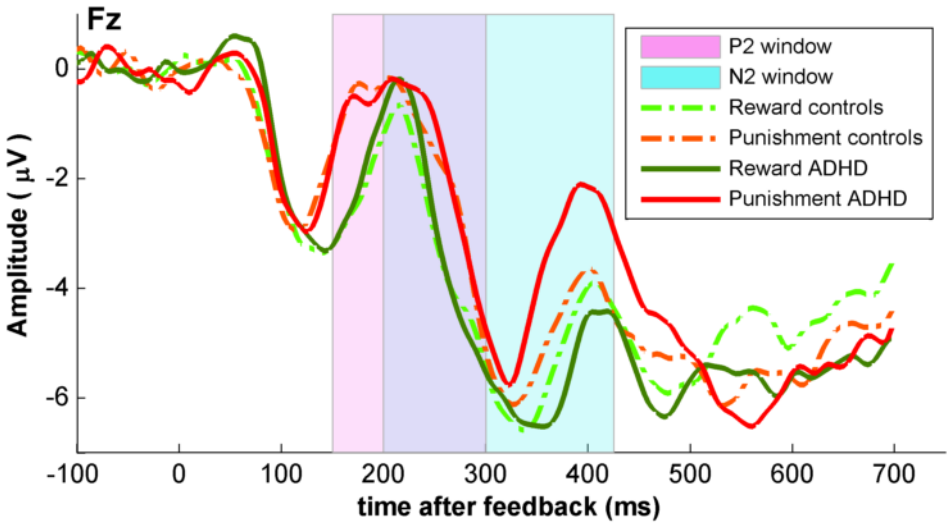

© 2014 American Medical Association. All rights reserved.

Downloaded From: http://archpsyc.jamanetwork.com/ by a ETH ZUERICH User on 04/22/2016

eFigure 2. Neural correlates of RPEs and decision function.

A, Increasing RPEs are associated with increased activation in a network containing the vmPFC and the sgACC/VS (p<.05 voxel-height FWE). B, Decreasing RPEs are associated with a network containing the anterior insula, mPFC and the dlPFC. The model parameter β, which indicates the steepness of the decision function, elicits a network containing the mPFC (C) and the latPFC (D) during the decision phase (p<.05 cluster-extent FWE).

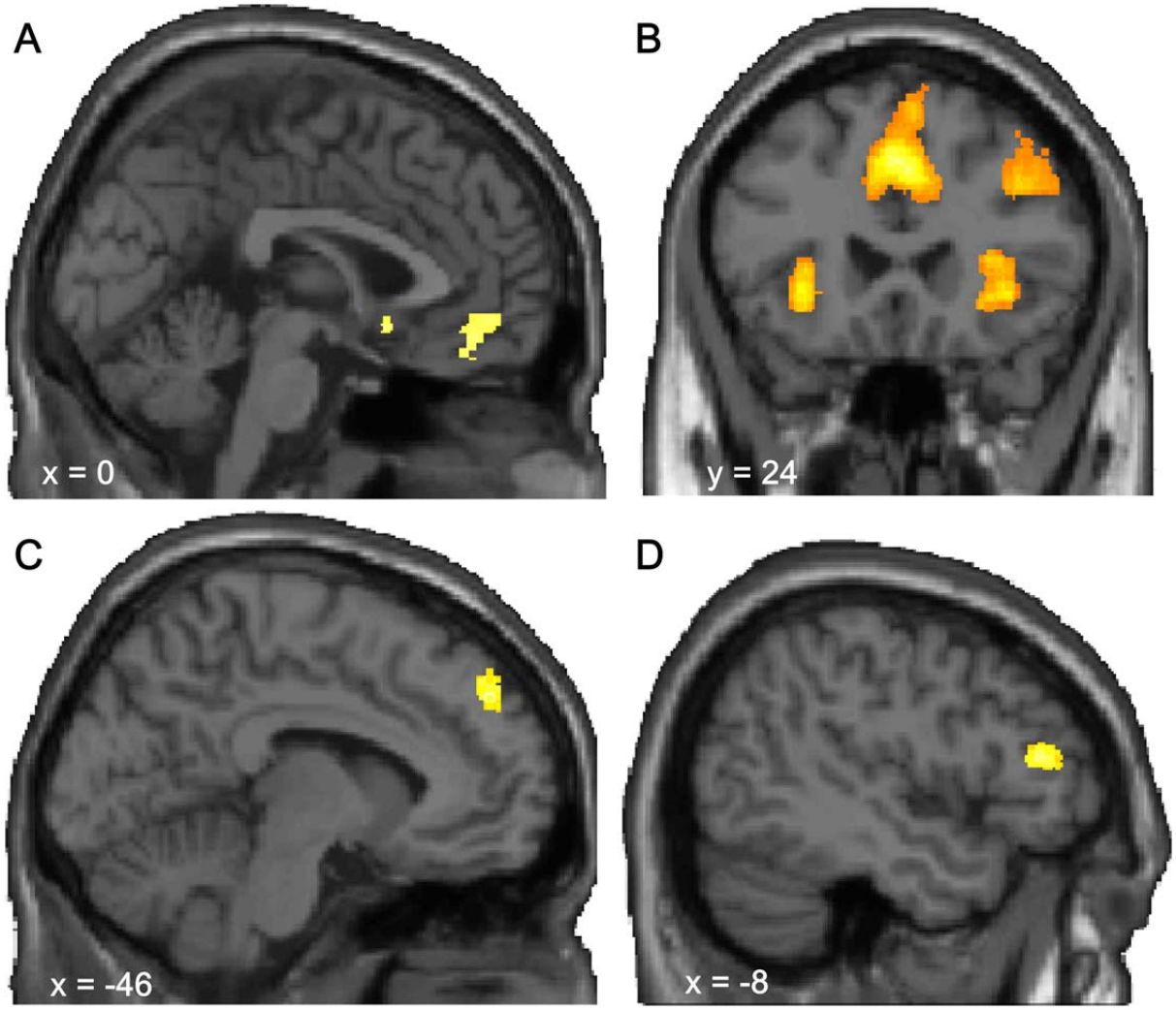

© 2014 American Medical Association. All rights reserved.

Downloaded From: http://archpsyc.jamanetwork.com/ by a ETH ZUERICH User on 04/22/2016

eFigure 3. Analysis of sgACC/VS-ROI and functional connectivity.

The analysis of a cluster in the subgenual ACC and ventral striatum (sgACC/VS) displayed no activation differences between the groups during cue-phase (A). However, during outcome phase (B), subjects with ADHD (red) showed no activation, while the healthy controls (black) showed normal modulation. The same held true when the ROI was based on the activation from an independent group of adults to analyze the RPE effects during cue (C) and outcome (D). (E) A functional connectivity analysis revealed a significant functional connectivity between the sgACC/VS-cluster and the mPFC (cluster derived from $RPE_{outcome}$ contrast between groups) in both groups. However, the functional connectivity was significantly decreased in ADHD compared to controls. * p < .05; ** p < .01; *** p < .001.

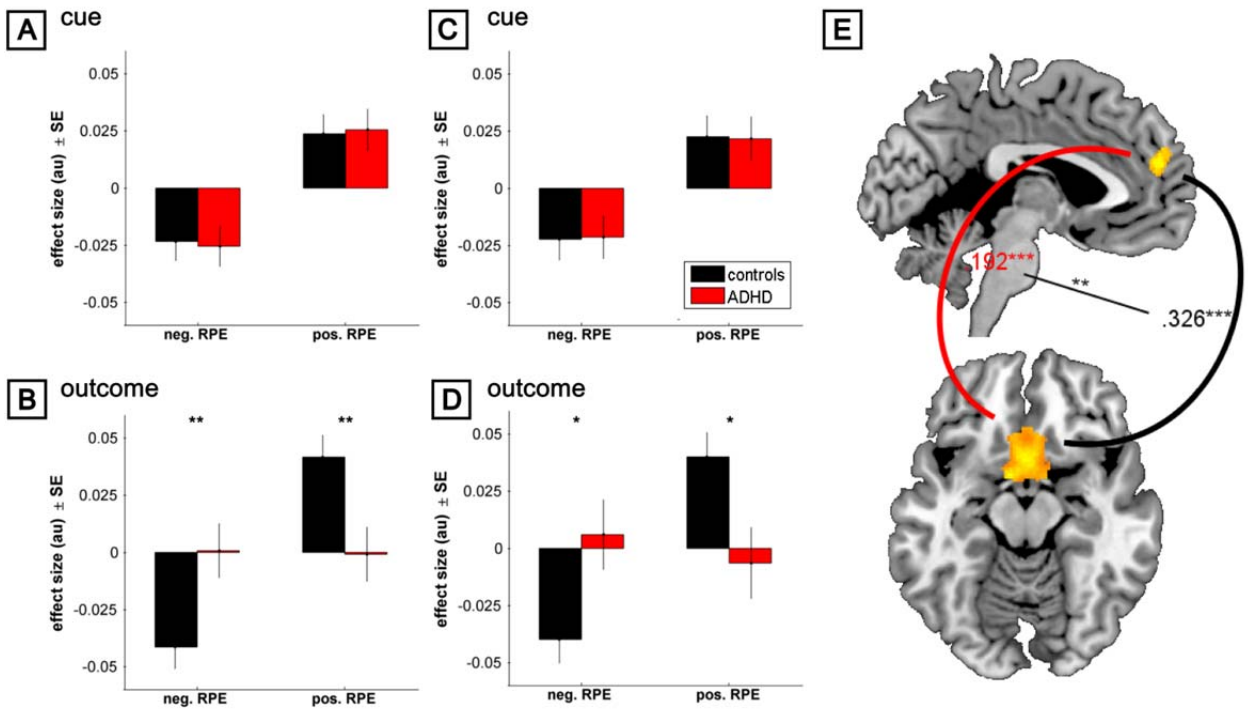

© 2014 American Medical Association. All rights reserved.

Downloaded From: http://archpsyc.jamanetwork.com/ by a ETH ZUERICH User on 04/22/2016

eTable 1. Behavioral differences between groups.

Analysis of reaction times and number of misses revealed no difference between the groups. This ensures that group differences found in modeling and earnings are not caused by reaction time differences between the groups (mean±std).

	controls	ADHD	
reaction time: mean	687ms±75	741ms±75	t(38)=1.43, p=.160
reaction time: standard deviation	178ms±37	197ms±44	t(38)=1.54, p=.132
misses	2.05±2.21	3.85±7.34	t(38)=1.05, p=.300

© 2014 American Medical Association. All rights reserved.

Downloaded From: http://archpsyc.jamanetwork.com/ by a ETH ZUERICH User on 04/22/2016

eTable 2. Results of the Bayesian model comparison.

The combination of the HGF learning model and the softmax decision model outperformed the other models for the whole group and for the healthy controls. For the ADHD patients, the anticorrelated Rescorla-Wagner model performed best. Please note that p_p and p_x sum up to 1 over the model space. Bold indicates the winning model. p_p: expected posterior probability; p_x: exceedance probability; RW: Rescorla-Wagner, sm: softmax decision model, usq: unit square decision model.

	all subjects		ADHD		controls	
models	p_p	p_x	p_p	p_x	p_p	p_x
anticorrelated RW - sm	.44	.30	.59	**.92**	.26	.02
anticorrelated RW - usq	.03	.00	.05	.00	.04	.00
HGF - sm	.51	**.70**	.32	.08	.66	**.98**
HGF - usq	.03	.00	.05	.00	.05	.00

© 2014 American Medical Association. All rights reserved.

Downloaded From: http://archpsyc.jamanetwork.com/ by a ETH ZUERICH User on 04/22/2016

eTable 3. Results of additional fMRI analyses: main task effect of RPE (cue + outcome) and decision steepness (model parameter β).

The RPEs elicit the typical activation found for RPE processing (regions reported at $p < .05$ voxel-height FWE, $k > 10$). Subjects with higher β show increased activations in these areas (regions reported at $p < .05$ cluster-extent FWE). Cluster size is given in number of voxels. Coordinates are reported in MNI space.

Contrast	Region	Hemisphere	Cluster size	x	y	z	z Score
$RPE_{cue+outcome}$	vmPFC	bilateral	435	-8	44	-12	6.38
	PCC	bilateral	373	-5	-55	19	6.37
	hippocampus/amygdala	right	21	15	-6	-20	5.85
			19	26	-16	-17	5.58
		left	18	-29	-19	-17	5.70
			12	-30	-34	-18	5.65
			12	-24	-24	-20	5.52
	latPFC	left	15	-51	32	7	5.74
	sgACC/VS	bilateral	20	0	14	-9	5.67
$-RPE_{cue+outcome}$	anterior insula	left	1035	-32	21	-8	>8
		right	1624	39	17	-6	>8
	mPFC	bilateral	3993	-6	27	39	>8
	latPFC	right	3451	26	53	-2	7.53
		left	773	-32	51	16	6.65
	IPL	right	1335	48	-45	40	7.14
			227	-39	-45	37	6.51
	precuneus	bilateral	420	8	-64	49	6.76
	caudate	left	118	-11	9	1	6.36
		right	238	15	18	1	6.33
	midbrain		202	-3	-24	-5	6.35
	thalamus	left	16	-11	-15	12	6.02
	dlPFC	left	39	-44	30	37	5.72
β	latPFC	right	197	63	15	9	4.75
		left	251	-48	35	12	4.44
	mPFC	bilateral	301	-8	48	37	4.56
	precentral	right	153	11	-25	73	4.48

© 2014 American Medical Association. All rights reserved.

Downloaded From: http://archpsyc.jamanetwork.com/ by a ETH ZUERICH User on 04/22/2016

			177	39	-15	33	4.13
	STG	right	125	59	-24	7	4.32
	dlPFC	left	92	-23	23	49	3.68

© 2014 American Medical Association. All rights reserved.

Downloaded From: http://archpsyc.jamanetwork.com/ by a ETH ZUERICH User on 04/22/2016